Sequence-Dependent Variations Associated with H2A/H2B Depletion of Nucleosomes

L. Kelbauskas,* N. Chan,*† R. Bash,*†‡ P. DeBartolo,† J. Sun,* N. Woodbury,*† and D. Lohr†
*Biodesign Institute, †Department of Chemistry and Biochemistry, and ‡Department of Physics and Astronomy, Arizona State University, Tempe, Arizona 85287

ABSTRACT Mechanisms that can alter nucleosome structure to enhance DNA accessibility are of great interest because of their potential involvement in genomic processes. One such mechanism is H2A/H2B release from nucleosomes; it occurs in vivo and is involved in the in vitro activities of several transcription-associated complexes. Using fluorescence approaches based on Förster resonance energy transfer, we previously detected sequence-dependent structure/stability variations between 5S and two types of promoter nucleosomes (from yeast *GAL10* or mouse mammary tumor virus promoters). Those variations included differing responses when nucleosomes were diluted to concentrations (sub-nM) known to produce H2A/H2B loss. Here, we show that treatment of these same three types of nucleosomes with the histone chaperone yNAP-1, which causes H2A/H2B release from nucleosomes in vitro, produces the same differential Förster resonance energy transfer responses, again demonstrating sequence-dependent variations associated with conditions that produce H2A/H2B loss. Single-molecule population data indicate that DNA dynamics on the particles produced by diluting nucleosomes to sub-nM concentrations follow two-state behavior. Rate information (determined by fluorescence correlation spectroscopy) suggests that these dynamics are enhanced in MMTV-B or *GAL10* compared to 5S particles. Taken together, the results indicate that H2A/H2B loss has differing effects on 5S compared to these two promoter nucleosomes and the differences reflect sequence-dependent structure/stability variations in the depleted particles.

INTRODUCTION

Nucleosomes are the basic units of eukaryotic chromosome structure. They consist of slightly less than two superturns of double-stranded DNA (~147 bp) wrapped around a histone octamer made up of one H3/H4 tetramer and two H2A/H2B dimers (1,2). The H3/H4 tetramer binds primarily to the central DNA region of the nucleosome, ~60 bp around the dyad. The H2A/H2B dimers each bind to ~30 bp DNA regions lying adjacent to this central region (Fig. 1; (2)). Eukaryotic genomes are extensively nucleosome covered (cf. (3,4)); coverage includes regulatory DNA sequences like promoters (5–7) and replication origins (8,9). Nucleosomes can restrict regulatory factor access to DNA. Thus, there is great interest in mechanisms that can produce nucleosomal DNA exposure, whether intrinsic or protein mediated (cf. (10)).

The nucleosome is a dynamic structure in both its DNA and histone components (10–13). For example, histones H2A/H2B undergo rapid exchange from nucleosomes in vivo (14) and H2A/H2B loss is associated with the in vitro action of many functional complexes such as RNA polymerase (15), transcription elongation (16), and ATP-dependent nucleosome remodeling complexes (17,18) and the histone chaperone yNAP-1 (19). Because each H2A/H2B dimer in the nucleosome interacts with a ~30 bp region of DNA, dimer removal should significantly enhance DNA accessibility, at least in parts of the nucleosome, while maintaining some histone presence (H3/H4).

Intrinsic variability in nucleosome properties could have a role in gene regulation in vivo (20). For example, nucleosomes with unique structure or stability properties could create chromatin sites with enhanced (or depressed) intrinsic DNA dynamics, thus affecting inherent accessibility of this DNA to regulatory factors, or enhanced (or depressed) ability to undergo the types of nucleosome transitions that might take place during functional processes, such as H2A/H2B loss. Nonallelic histone variants are an example of a nucleosome feature that could create unique chromatin regions of functional significance; variants are found in distinct chromosomal locations (10,21), associated with diverse processes, and their presence can produce structurally distinct nucleosomes (22–24). DNA sequence-dependent variations in nucleosome structure and stability are another potential source of functionally important differences. Sequence-dependent variations have been observed in various nucleosome features, including reconstitution efficiencies (25–27), repositioning tendencies and remodeling (28,29), DNA torsional and dynamic properties (30), stability features (31,32), ligand interactions (33,34), and acetylation effects (35). However, the absence of an experimental approach with enough sensitivity to detect fundamental sequence-dependent nucleosome conformational differences for a wide range of intrinsic features has hampered progress in this area.

Förster resonance energy transfer (FRET) is a powerful and sensitive approach for the study of conformational features in biological macromolecules. Energy transfer (FRET)

Submitted May 1, 2007, and accepted for publication August 6, 2007.

Address reprint requests to D. Lohr, Dept. of Chemistry and Biochemistry, Arizona State Univ., Tempe, AZ 85287-1604. Tel.: 480-965-5020; Fax: 480-965-2747; E-mail: dlohr@asu.edu.

Editor: Alberto Diaspro.

0006-3495/08/01/147/12 $2.00

doi: 10.1529/biophysj.107.111906

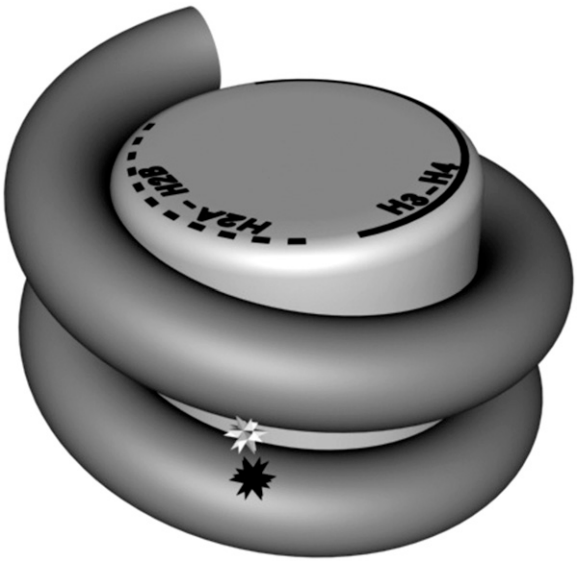

FIGURE 1 The labeled nucleosome. DNA is labeled with fluorophores (Cy3 and Cy5) at positions 80 bp apart bracketing the center of the fragment. Reconstitution into nucleosomes brings the fluorophores (indicated by *stars*) close together, providing efficient energy transfer. The DNA fragment is chosen and fluorescently labeled so that the reconstituted nucleosome will lie in the major nucleosome positioning frame determined for that sequence (see Materials and Methods; (42)) and the fluorophores will lie within the nucleosome 25–40 bp from each nucleosome terminus. The example shown here is for the MMTV-B nucleosome in which each fluorophore lies just over 30 bp from a nucleosome terminus (based on the known nucleosome position on that sequence (47,64). The DNA segments of the intact nucleosome that bind to the H3/H4 tetramer (*solid line*) or an H2A/H2B dimer (*dotted line*) in the top half of the nucleosome are indicated schematically on the top of the disk (based on Luger et al. (2)).

occurs when an excited donor fluorophore is in proximity (typically 1–5 nm) to an appropriate acceptor fluorophore. The sixth power dependence of FRET efficiency on fluorophore separation makes FRET very sensitive to distance changes between the donor and acceptor, such as those occurring during conformational transitions. FRET approaches can monitor intrinsic or protein-induced conformational changes at bulk and single-molecule levels, and FRET-based methods have been used in chromatin studies (22,23,36–41).

Using a FRET-based approach, we recently observed some significant DNA sequence-dependent variations in nucleosome structure and stability features (42). Our approach involves labeling a DNA fragment (~160 bp) with the donor fluorophore, Cy3, and acceptor fluorophore, Cy5, at sites 80 bp apart, bracketing the center of the fragment (43). When this labeled DNA is reconstituted into nucleosomes, the donor and acceptor are brought into proximity by the nucleosomal DNA wrap (Fig. 1), allowing efficient excitation energy transfer from Cy3 to Cy5 and producing a strong FRET signal (43). Nucleosome conformational changes can be detected as changes in the FRET efficiency, usually decreases. This system has provided information on basic structural features such as diffusion coefficients or intrinsic FRET efficiencies and has proven to be a sensitive monitor of conformational changes produced in response to salt, modest temperature change, or dilution, all of which reflect nucleosome stability features (42,43).

Our previous work (42) compared the structure and stability properties of nucleosomes reconstituted on three natural DNA sequences. Two of these were from promoters: a TATA-containing sequence from yeast *GAL10* (44) or a sequence containing four of the six glucocorticoid receptor response elements from the MMTV promoter (45). These promoter sequences were chosen for study because in vivo the sequences reside in nucleosomes that undergo significant and functionally important structural changes during transcription activation (44,45). The third sequence, 5S rDNA, has been widely used for in vitro chromatin studies (46) and provided a standard of comparison. All three sequences are known to position nucleosomes (44,47–49), and all three reconstituted in one main occupied position (42).

Significant structure and stability variations between 5S and the two types of promoter nucleosomes (*GAL10* or MMTV-B) were detected (42). For example, differing FRET responses were observed when these nucleosomes were diluted to concentrations that have been shown to provoke major H2A/H2B release (50), suggesting variations associated with H2A/H2B loss. Here, treatment with the histone chaperone yNAP-1, which provides a very different method of producing H2A/H2B release from nucleosomes (19), is shown to yield the same differential FRET responses as in the dilution studies (decreases for MMTV-B and *GAL10* but not 5S). This finding greatly strengthens the conclusion that the FRET differences caused by dilution reflect variations associated with H2A/H2B loss. Single-molecule detection techniques are used to characterize the 5S, MMTV-B, and *GAL10* particles produced at low (100–200 pM) concentrations, and fluorescence correlation spectroscopy (FCS) approaches are used to study intrinsic DNA dynamics on these particles.

MATERIALS AND METHODS

DNA and nucleosome preparation

Fluorescently labeled dsDNA fragments (~160 bp in length) were made by polymerase chain reaction techniques (43), using various templates and the appropriate, labeled primers, as described in detail previously (42). The *GAL10* fragment (206–365 bp from an *Eco*RI site (cf. (44)) corresponds to the in vivo position of a TATA-containing nucleosome. The MMTV-B fragment (−70 to −230 bp on the promoter (51)) corresponds to the in vivo position of nucleosome B (47). The sea urchin 5S rDNA fragment is the 5′ *Eco*RI-Ban II region (49).

Labeled DNA is gel purified then reconstituted into nucleosomes using purified HeLa histone octamers as described previously (42,52). The histone octamers were prepared as described in Yodh et al. (53) and were a generous gift from Dr. J. Yodh. For some studies, the mononucleosome band was eluted from (unstained) gels by excising a gel slice containing the band and placing the slice in TE buffer pH 8 at room temperature for 12–24 h.

Nucleosome response to yNAP-1

Nucleosomes (10 nM concentration) were treated with yNAP-1 protein (10 nM monomer concentration) in TE buffer (10 mM Tris and 1 mM EDTA, pH 8), containing 1 mM dithiothreitol. FRET efficiency was measured (see below) immediately after the addition of the yNAP-1 to the sample (time ''0'') and at 15–30 min intervals afterward. The yNAP-1 was a generous gift from Y. Park and K. Luger; it functions as a dimer under these conditions ((19); K. Luger, Dept. of Chemistry and Biochemistry, Colorado State University, personal communication, 2007).

Single-molecule distributions and salt dependence

Single-molecule FRET measurements were conducted using an experimental setup described in Kelbauskas et al. (42). Briefly, a microscope (ECLIPSE TE2000-U, Nikon, Melville, NY) operated in a confocal configuration and equipped with an oil immersion objective lens (100×, numerical aperture = 1.4) was utilized. The excitation source was a continuous wave frequency-doubled Neodymium-doped yttrium vanadate ($Nd:YVO_4$) laser (Millenia Xs, Coherent, Santa Clara, CA) operating at 532 nm. The photons in Cy3 and Cy5 spectral emission channels were detected with silicon avalanche photodiodes (SPCM-AQR-12, Perkin Elmer, Fremont, CA) using appropriate emission filters (BP570/40 for Cy3 and BP670/40 for Cy5 detection channel; Chroma Technology, Rockingham, VT) placed in front of each detector. FRET efficiency was calculated using the following equation:

$$E_{\mathrm{FRET}} = \frac{I_{\mathrm{A}}}{I_{\mathrm{A}} + \gamma I_{\mathrm{D}}}, \tag{1}$$

where I_{A} and I_{D} are the fluorescence intensities measured in the acceptor and donor channel, respectively, and $\gamma = 1.12$ is a factor correcting for the cross talk between the detection channels and any contribution from direct excitation of the acceptor. E_{FRET} errors were calculated as the mean ± SE using $\Delta E_{\mathrm{FRET}} = \frac{\sigma}{\sqrt{N}}$, where σ is the standard deviation and N is the number of independent measurements.

The salt-dependence measurements were carried out in TE buffer, pH 8, at increasing concentrations of NaCl, achieved by stepwise addition of 1 μl aliquots of 500 mM NaCl to the sample. After each addition, 5–10 min were allowed for equilibration before measurement.

Fluorescence correlation spectroscopy measurements

FCS measurements were carried out using the experimental setup as described above and samples diluted to ~200 pM. Correlation curves were measured using a hardware dual-channel digital correlator card with a sampling time of 12.5 ns (Flex2k-12x2; Correlator, Bridgewater, NJ) and the vendor's software. Data analysis and fitting were performed using locally written software based on LabView.

Calculation of conformational dynamics parameters

For molecules labeled with a FRET pair-like Cy3 and Cy5, the emission intensity fluctuations in the donor (Cy3) or acceptor (Cy5) detection channel can be caused by two different kinds of processes (assuming that there are no photophysical effects, like intersystem crossing to the triplet state, and that photobleaching can be neglected): fluctuations due to the diffusion of molecules through the excitation volume; and fluctuations due to conformational transitions that result in changes in the energy transfer efficiency. Applying the formalism described in Magde et al. (54), Berne and Pecora (55), Krichevsky and Bonnet (56), and Bonnet et al. (57) adapted to our specific model system (see Supplementary Material), we were able to determine conformational dynamics parameters of particles. As required, our system exhibits two-state behavior (see below).

RESULTS

The three fluorescently labeled DNA sequences used in this work, *GAL10*, MMTV-B, or 5S, were shown to reconstitute into typical nucleosome structures, based on polyacrylamide gel and salt stability analyses (common diagnostics for reconstituted nucleosome samples (58–60)), with little evidence of nucleosome positioning heterogeneity; one occupied position was observed for each (42). Despite these general similarities, a number of structure and stability differences between 5S and MMTV-B or *GAL10* nucleosomes were detected. Since all three types of nucleosomes were reconstituted and analyzed in the same way (same histones etc.), the differences must reflect DNA sequence-dependent variations.

The FRET response differences observed when nucleosomes were diluted to sub-nM concentrations were of particular interest. FRET efficiencies were more or less constant down to ~2 nM for all three types but then decreased steadily with further dilution for MMTV-B and *GAL10* but actually increased slightly for 5S nucleosomes. Studies using radiolabeled histones have shown that major H2A/H2B release occurs as reconstituted nucleosomes are diluted to nM concentrations (50). Thus, these FRET response differences suggested that there are variations associated with H2A/H2B release among the three types. The *GAL10* and MMTV-B FRET decreases were only partial (10%–30%), even at the highest dilutions (42). Partial decreases are consistent with partial changes, such as H2A/H2B release, in internally labeled nucleosomes (our probes bracket an 80 bp distance across the central region of the nucleosome (Fig. 1) (42). The H3/H4 tetramer, which remains bound to DNA (50), provides sufficient DNA wrapping to keep the probes close enough for significant energy transfer.

Treating nucleosomes with yNAP-1

To obtain an independent test of the possible relationship between H2A/H2B release and FRET response differences among these three types of nucleosomes, we treated all three with the yeast histone chaperone yNAP-1, which has been shown to efficiently remove H2A/H2B from nucleosomes in vitro (19). Substoichiometric concentrations of yNAP-1 (0.5 mol of yNAP-1 dimer per mole of nucleosomes) were used to minimize nonspecific effects, and nucleosome concentrations (~10 nM) were well above those at which we observe concentration dependent FRET decreases (42). Thus, the substrates for yNAP-1 should be intact nucleosomes. FRET was monitored for up to 3 h at room temperature.

Fig. 2 *a* shows typical response curves for the three types of treated nucleosome samples. FRET efficiencies from 5S samples (*solid squares*, *solid line*) are constant, but *GAL10*

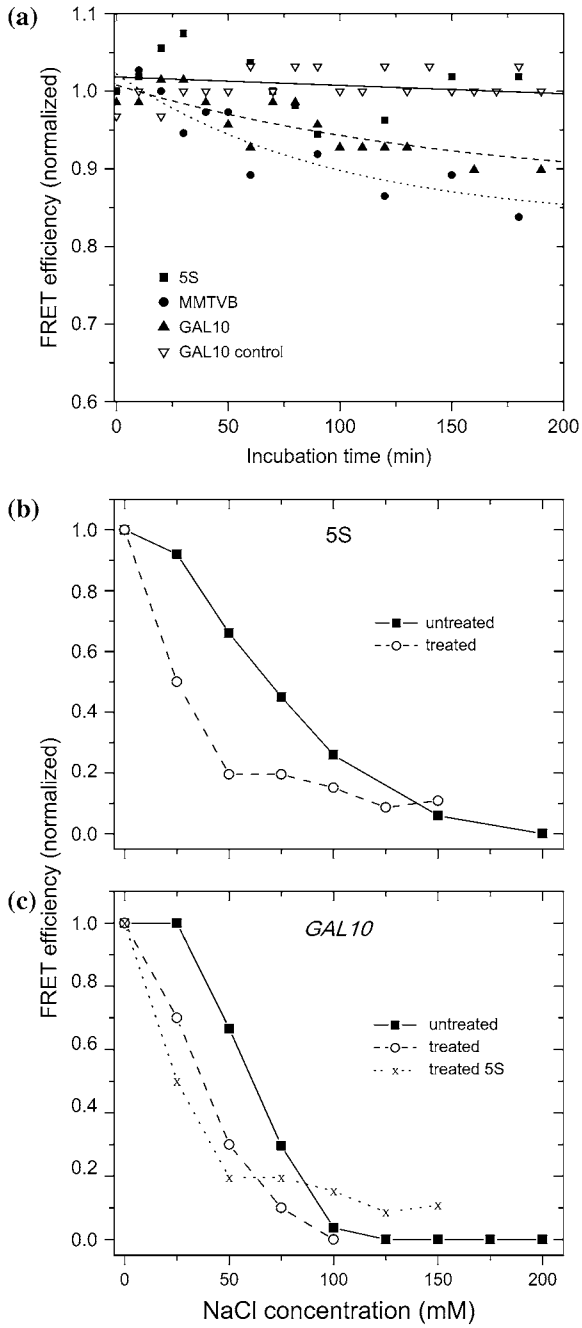

FIGURE 2 Treating nucleosomes with *yNAP-1*. In panel *a*, the FRET efficiency of nucleosome samples is plotted as a function of incubation time with yNAP-1. yNAP-1 was present at ratios of 0.5 mol yNAP-1 dimer per mole of nucleosomes (nucleosome concentration 10 nM). The response of treated 5S (*solid squares, solid line*), MMTV-B (*solid circles, dotted line*), or *GAL10* (*solid triangles, dashed line*) nucleosome samples are shown. The response of a sample (*GAL10*) incubated under the same conditions but without yNAP-1 is also shown (*open inverted triangles*). 5S and MMTV-B samples also show no FRET efficiency changes in the absence of yNAP-1 (data not shown). The lines are least-square fits (linear or polynomial) to the data points. Panels *b* and *c* show salt titrations, plots of FRET efficiency as a function of NaCl concentration, for 5S (*panel b*) or *GAL10* (*panel c*) samples without yNAP-1 treatment (*solid squares, solid lines*) or after yNAP-1 treatment as described in panel *a* (*open circles, dashed lines*). The lines are simply drawn to connect the points as an aid in visualization. The curve traced out by ''x'' in panel *c* is the curve for treated 5S samples (*panel b*), included again here for ease of comparison of 5S and *GAL10* responses.

(*solid triangles*, *dashed line*) and MMTV-B (*solid circles*, *dotted line*) samples show a time-dependent decrease in FRET efficiency. After ~3 h of incubation, the FRET efficiency in MMTV-B and *GAL10* samples has decreased by 10%–15%, whereas that from 5S nucleosomes remains essentially unchanged. In the absence of yNAP-1, the FRET efficiency in such incubated samples remains constant for all three types of samples (cf. *GAL10* nucleosomes, *open inverted triangles*). Thus, yNAP-1 treatment reduces the FRET efficiency of MMTV-B and *GAL10* but not 5S nucleosomes. The precise level of the FRET decrease for MMTV-B and *GAL10* samples varies by 3%–5% (mean ± SE of two to three experiments; see Materials and Methods), as might be expected under these relatively dilute conditions; but the clear qualitative behavioral difference, decreasing FRET for yNAP-treated MMTV-B or *GAL10* but not 5S nucleosome samples, is a constant feature.

To check whether yNAP-1 was actually acting on the 5S nucleosomes, we carried out salt titrations of 5S samples that had been treated as above with yNAP-1. H2A/H2B absence makes the nucleosome more salt sensitive (N. Chan and L. Kelbauska, unpublished observations). Therefore, the salt stability of yNAP-1-treated 5S nucleosomes should be lower than the stability of untreated 5S nucleosomes if yNAP-1 treatment has caused H2A/H2B release. This is the case (Fig. 2 *b*). The yNAP-1-treated 5S nucleosome samples (*open circles*, *dashed line*) are more salt sensitive, i.e., their structure is disrupted (the FRET efficiency decreases) at lower NaCl concentrations than for untreated 5S samples (*solid squares*, *solid line*). Therefore, yNAP-1 is acting on 5S nucleosomes even though their FRET efficiencies do not change and that action produces changes (lower salt stabilities) that are consistent with H2A/H2B removal. yNAP-1 treatment also decreases the salt stabilities of *GAL10* (Fig. 2 *c*) and MMTV-B (data not shown) nucleosomes to very similar levels as that of yNAP-treated 5S nucleosomes (cf. Fig. 2 *c*, ''x'' curve versus *dashed line*). Thus, yNAP-1 appears to be acting more or less equally, i.e., depleting H2A/H2B to similar extents, on all three types of nucleosomes.

It is important to note that these three types of nucleosomes have salt stabilities that are much higher at bulk concentrations (42) and similar to the salt stabilities shown for other types of nucleosomes under bulk conditions (22,60). However, stability is lower at these (10 nM) nucleosome concentrations. Thus, lower salt concentrations can produce destabilization (and FRET changes) in these experiments than at bulk nucleosome concentrations. Importantly, the relative stability differences noted between these three, 5S > *GAL10* > MMTV-B, are the same at bulk (42) or these lower concentrations (compare ''untreated'' nucleosomes, Fig. 2, *b* and *c*, data not shown). Also, controls to test the effects of

salt on fluorescence properties of Cy3 and Cy5 dyes (using singly labeled nucleosomes) have demonstrated that differential salt effects on FRET efficiency are negligible in this system (42).

We also carried out treatments with yNAP-1 present in excess, to try to estimate the extent of FRET loss achievable from MMTV-B and *GAL10* nucleosomes. The average (multiple experiments) FRET decreases produced by high yNAP-1 concentrations (2–4 molar yNAP-1 excess) are roughly similar to the decreases observed when nucleosomes are diluted to sub-nM concentrations (data not shown): ~10% for MMTV-B nucleosomes by dilution or by NAP-1 treatment; and ~30% (dilution) versus ~20% (yNAP-1 treatment) for *GAL10* nucleosomes. Quantitative similarities are consistent with both treatments causing the same type of change, namely H2A/H2B loss from nucleosomes. In sum, these yNAP-1 experiments provide independent and compelling evidence that effects associated with H2A/H2B release produce differing FRET responses in 5S compared to the two types of promoter nucleosomes, thus strengthening the similar conclusion from nucleosome dilution studies. The results also demonstrate directly that 5S nucleosomes show no FRET change when H2A/H2B depleted.

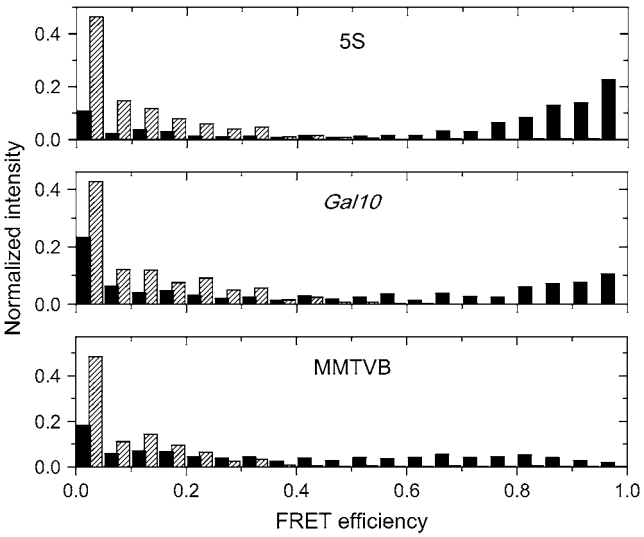

FIGURE 3 Single-molecule FRET efficiency population distributions. Mononucleosomes were eluted from gels, diluted to 0.2 nM concentration, and the FRET efficiencies of individual molecules in the sample were determined in solution. Distributions of FRET efficiency for 5S (*top panel*), *GAL10* (*middle panel*), and MMTV-B (*bottom panel*) particles are shown, with FRET efficiency plotted on the *x* axis and the normalized frequency (normalized to the total number of individual molecules observed in the experiment) plotted on the *y* axis. The solid bars show results obtained in low salt; the hatched bars show results obtained in 200 mM NaCl.

Single-molecule distributions

Some of our previous studies (42) were carried out at sub-nM concentrations. Based on prior results (50), the yNAP-1 results above, and results presented below, nucleosomes are likely to be H2A/H2B depleted at these concentrations and will thus be referred to as ''particles''. H2A/H2B-depleted nucleosomes (particles) are of intrinsic interest (see Introduction), so we turned to single-molecule techniques to compare the properties of the particles produced by dilution of 5S, MMTV-B, and *GAL10* nucleosomes.

Single-molecule population distributions can provide insights into specific features that are hidden in ensemble average results. To eliminate contributions from free DNA and higher molecular weight material that may be present in reconstituted samples (42), the samples were run on gels and the mononucleosome band was eluted (see Materials and Methods). The eluted mononucleosomes were diluted to 0.2 nM concentrations, and single-molecule counting was carried out in solution (Fig. 3). The features described below are also characteristic of single-molecule distributions from noneluted samples (data not shown) and therefore do not result from effects associated with elution. For the sake of discussion, the distributions will be divided into three regions: high (0.8–1.0), low (0–0.2), and midrange (0.2–0.8) FRET efficiency. High efficiency molecules maintain their fluorophores close enough for major energy transfer, whereas in low efficiency molecules, the fluorophores are too far apart for significant energy transfer. Molecules in the midrange of the distribution fall between these two extremes. Based on the R_o value, the distance at which energy transfer is 50% (5–6 nm for Cy3/Cy5 probes, Amersham Biosciences, Buckinghamshire, UK), FRET efficiencies of 0.8–1.0 (high efficiency molecules) or 0–0.2 (low efficiency molecules) would correspond to average probe separations of <4 nm or >7 nm.

Distributions for 5S particles contain a significant population of molecules with efficiencies ≥ 0.8 (Fig. 3, *top panel*, *solid bars*), whereas *GAL10* (*middle panel*, *solid bars*) and MMTV-B (*lower panel*, *solid bars*) distributions show fewer such molecules. Thus, the relative fraction of particles that maintain their FRET labels very close to each other, on average, is larger in 5S than in MMTV-B or *GAL10* populations. These population differences are consistent with the higher average FRET efficiencies noted for 5S compared to MMTV-B or *GAL10* particles (sub-nM concentrations) or nucleosomes (bulk concentrations) (42).

All three distributions contain significant numbers of molecules with low FRET efficiencies (0–0.2) but the relative fraction of these molecules is higher in the MMTV-B and *GAL10* distributions (Fig. 3, *solid bars*). None of the three distributions shows a major population at any FRET efficiency in the midrange (0.2–0.8). In all cases, the individual frequency values, i.e., the frequency of molecules with a given efficiency, are much lower in this midrange of the distribution than at very high (0.8–1.0) or very low (0– 0.2) FRET efficiencies. A distribution in which molecules tend to have either very low or very high FRET efficiencies suggests

that molecules reside mainly in one of two conformational states: a state in which DNA associates with the particle such that the fluorophores are, on average, close enough to produce strong energy transfer (0.8–1.0); and a state in which the fluorophores are, on average, too far apart for significant energy transfer to occur, which results in low (0–0.2) FRET efficiency. Each of these states must be stable for time periods that are long in comparison to the average time it takes a molecule to diffuse across the excitation volume (see also below).

To confirm that the high FRET efficiency molecules reflect energy transfer occurring in structured complexes, single-molecule distributions were obtained for the same samples in 200 mM NaCl, which under these conditions is sufficient to destabilize the particles and abolish energy transfer (see below). This treatment completely removes the high (and intermediate) FRET efficiency molecules from all three distributions, leaving only low efficiency molecules (Fig. 3, all *panels*, *hatched bars*). Thus, the high efficiency molecules observed in the low salt distributions (Fig. 3, *solid bars*) must reflect stable, structured complexes in which Cy3 and Cy5 are on average close enough for very efficient energy transfer. The loss in the intermediate FRET efficiency ranges shows that these low-abundance molecules also are structured complexes. Their lower FRET efficiencies could reflect a less well-folded and/or a more dynamic structure. Intermediate efficiencies could also result from complexes that happened to change conformation (high to low FRET or vice versa) while passing through the beam, although our FCS results (see below) suggest that the probability of such an event is $<$1–2 per 100 molecules.

There is some sample-to-sample variation in these single-molecule distributions, but the major features, and the differences between 5S and MMTV-B or *GAL10* samples, are consistently observed. For example, the fraction of high efficiency molecules (0.8–1.0) in MMTV-B or *GAL10* samples never reaches 0.4, whereas the fraction in 5S samples is never below 0.5. Also, frequency values in the midrange of the distribution are always small relative to the values for low and high efficiency molecules, for all three types of samples.

Salt titrations at the single-molecule level

To study the detailed response of these three types of particles to salt treatment at the single-molecule level, single-molecule population distributions were obtained at various NaCl concentrations (cf. Fig. 4 *a*). Again, we note that destabilization and FRET changes occur at lower salt concentrations in particles at these sub-nM concentrations (L. Kelbauskas and N. Chan, unpublished observations) than under bulk conditions (42).

As NaCl concentration increases, the relative numbers of molecules with high ($\geq$0.8) FRET efficiencies progressively decrease and the numbers of molecules with very low FRET efficiencies progressively increase. At NaCl concentrations $>$100 mM, the very high efficiency molecules are largely gone and very low efficiency molecules strongly dominate the distribution. Most importantly, there is no significant

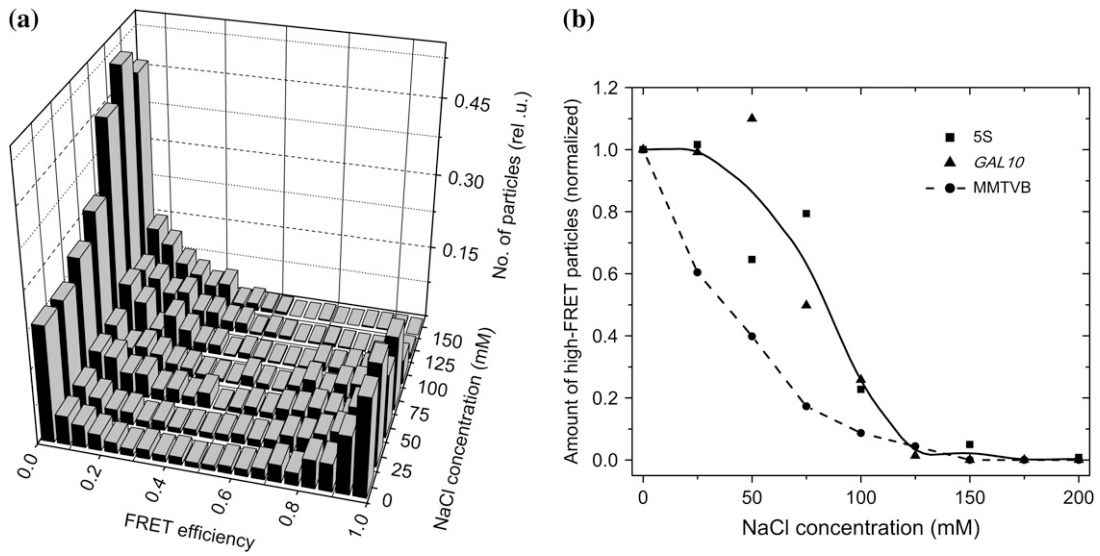

FIGURE 4 Salt-dependent responses at the single-molecule level. In panel *a*, single-molecule FRET efficiency distributions (cf. Fig. 3) for 5S samples at 0.2 nM concentration were determined at several NaCl concentrations. The FRET efficiency is shown on the *x* axis, the salt concentrations at which each distribution was obtained is shown to the right, and the vertical axis shows the number of particles (in relative units). Each distribution is normalized against the total number of events observed at that salt concentration to allow comparisons of distributions at various NaCl concentrations. This is a different 5S sample than the one shown in Fig. 3. In panel *b*, the normalized fractions of very high efficiency molecules (efficiency $\geq$0.9) present in a distribution are plotted versus NaCl concentration for 5S (*solid squares*), *GAL10* (*solid triangles*), and MMTV-B (*solid circles, dashed line*). The solid line is a fit to both the 5S and *GAL10* data, which are basically indistinguishable.

accumulation of species in the midrange, from 0.2–0.8 FRET efficiency, at any salt concentration; the frequency values in this range remain low throughout the salt titration except for a slight increase in the relative fraction of molecules in the 0.2–0.3 efficiency range at the higher NaCl concentrations. MMTV-B and *GAL10* distributions undergo similar profile changes with increasing salt concentrations; high efficiency molecules disappear, low efficiency molecules accumulate, including an enhancement of molecules in the 0.2–0.3 FRET efficiency range at the higher salt concentrations, and there is never a significant accumulation of species in the midrange (data not shown).

The relative fractional loss of high FRET efficiency (0.8–1.0) molecules from the 5S distribution between 0 and 200 mM NaCl is similar to the relative fractional gain of low efficiency molecules (0–0.2) over this range of salt, 0.56 vs. 0.61 (Table 1). The small difference undoubtedly reflects the conversion of molecules from intermediate to low efficiencies as the former are disrupted by salt. A decrease in high efficiency molecules, a parallel increase in low efficiency molecules, and no significant accumulation of molecules with intermediate FRET efficiencies is again indicative of a two-state response; the 5S particle exists mainly in either a folded (high FRET) or unfolded (low FRET) state and equilibrium is shifted toward the low FRET state with increasing NaCl concentration. Qualitatively similar results are obtained with MMTV-B and *GAL10* samples (Table 1).

The two-state behavior observed for the 5S particles (sub-nM concentrations) is more consistent with the behavior expected for H2A/H2B-depleted nucleosomes than for intact nucleosomes. The nucleosome has a tripartite organization, two H2A/H2B dimers, and one H3/H4 tetramer (1,2) and is known to dissociate in stages rather than in an all-or-none, two-state process. For example, salt addition causes the preferential release of H2A/H2B from nucleosomes; H3/H4 tetramer-DNA dissociation occurs at distinctly higher salt concentrations (cf. (22)). Thus, if the 5S complexes at these sub-nM concentrations were intact nucleosomes, they would first lose H2A/H2B as salt is added. Based on the FRET response seen with MMTV-B and *GAL10* nucleosomes when H2A/H2B are released (by treatment with yNAP-1 or dilution to sub-nM concentrations), this loss should produce an initial partial FRET efficiency decrease for the 5S complexes. A partial FRET decrease in a substantial proportion of molecules ought to be reflected in the 5S single-molecule distributions. Specifically, the high FRET efficiency peak should shift to lower but still significant efficiency values as H2A/H2B are released and then fall to very low values as the depleted particles are completely disrupted by salt. However, there is no evidence of such a peak shift in the 5S data. Thus, this two-state behavior also suggests that 5S complexes are H2A/H2B-depleted at these sub-nM concentrations.

TABLE 1 Single-molecule population data

Particle Type	[NaCl] (mM)	Low FRET*	Intermediate FRET†	High FRET‡
5S	0	0.19	0.23	0.57
	200	0.80 (+0.61)§	0.19	0.01 (−0.56)§
MMTV	0	0.38	0.30	0.32
	200	0.83	0.16	0.01
GAL10	0	0.38	0.30	0.32
	200	0.74	0.26	0.0

Data are taken from Fig. 3.
*Fraction of molecules with FRET efficiencies from 0 to 0.2.
†Fraction of molecules with FRET efficiencies from 0.2 to 0.8.
‡Fraction of molecules with FRET efficiencies from 0.8 to 1.0.
§The difference between the fraction present in 0 vs. 200 mM NaCl.

We do see evidence for distinct subpopulations of molecules in other states but only under particular conditions. For example, in the salt studies above, the relative fractional increase of molecules in the 0.2–0.3 FRET efficiency range at higher NaCl concentrations (cf. Fig. 4 *a*) suggests that a new state (structural or dynamic) might be available at these salt concentrations for all three types of particles. However, it remains a fairly minor component in the total population. As another example, raising the temperature to ~40°C causes a reversible, 10%–15% FRET efficiency increase in 5S (but not MMTV-B or *GAl10*) particles at sub-nM concentrations (42), but these particles have a lower salt stability (data not shown). This implies that at ~40°C, 5S particles are in a state with a lower average donor-acceptor separation, leading to higher FRET, but a lower salt stability than at room temperature.

Particles with FRET efficiencies from 0.9 to 1.0 represent the molecules in each population that show the most efficient energy transfer, i.e., the particles that are able to keep their fluorophores closest to one another, statically and dynamically. How does the salt stability of this specific class of molecules compare for the three types? The data in Fig. 4 *b* show that these very high FRET *GAL10* and 5S particles have similar salt stabilities, whereas MMTV-B very high FRET particles are clearly less salt stable. Thus, 5S populations contain relatively more of these very high FRET particles than *GAL10* populations (Fig. 3), but the two types of particles have similar structural stabilities (Fig. 4 *b*), at least as measured by salt sensitivity. On the other hand, 5S and MMTV-B differ both in the relative numbers of these molecules in the population and in their salt sensitivities. These results suggest that there may be a diversity of sequence-dependent variations in individual nucleosome properties, detectable with a sensitive approach such as this one. Interestingly, the low salt stability demonstrated by these very high FRET MMTV-B particles (Fig. 4 *b*) is also observed in salt titrations of MMTV-B nucleosomes (42). This suggests that this feature may be implemented largely via the H3/H4 tetramer.

Nucleosome dynamics

Opening-closing kinetics measured by FCS

The above-described variations in behavior among these three types of particles could arise from static or dynamic

differences. To gain insight into this issue, we investigated the rates of interconversion between the low-FRET and high-FRET states for all three types of particles at these sub-nM concentrations, using FCS approaches. The high-FRET state will be referred to as the ''closed'' state, a conformation(s) in which the FRET probes are very close together, on average, and the low-FRET state will be referred to as the ''open'' state, a conformation(s) in which the probes are too far apart for efficient energy transfer to occur. Rate constants that describe the time dependence of the transition between the two states will be determined. These constants undoubtedly reflect some sort of DNA association-dissociation dynamics on the particle, as reflected by FRET (donor-acceptor separation) changes, but the exact nature of the transition(s) occurring is unknown. This analysis will yield values for the average time a particle spends in each state, probably the most biologically relevant information.

Preliminary solution FCS measurements on these particles indicated that diffusion and conformational changes occur on different timescales: ~0.1 ms and ~10 ms, respectively (L. Kelbauskas and N. Chan, unpublished results). Diffusion time corresponds to the average time a particle spends in the excitation volume. Because the diffusion time is considerably shorter (~0.1 ms) than the average time for a conformational change to occur (~10 ms), the autocorrelation signal in these experiments will be dominated by intensity changes due to particle diffusion. Variations resulting from conformational changes do appear in the correlation signal but at longer delay times where the signal/noise ratio is low. This makes it difficult to recover conformational change information from the correlation data. We circumvented this problem by embedding the particles (at sub-nM concentrations) in 3% (w/v) agarose gels, thus slowing down their movements and increasing the diffusion times. Using this approach, average diffusion times are comparable to the rates of conformational change, i.e., in the 1–10 ms range, for all three types of particles. Note that our goal in this work is to obtain relative values of these parameters for the three types of particles.

Fig. 5 *a* shows the raw data and Fig. 5 *b* the normalized data and a fit to those data (using Eq. S4, Supplementary Material) for an FCS experiment carried out with MMTV-B particles in gels. To determine separate values for the open and closed states, equilibrium constants for particle formation must be known, then the kinetic values can be calculated (see Supplemental Material). Particle equilibrium constants K_{eq} were calculated from an independent experiment where the donor and acceptor emission sum intensities were measured in the corresponding detection channels at sub-nM particle concentrations and corrected for channel cross talk and direct acceptor excitation.

5S particles have larger equilibrium constants for the formation of the closed state than MMTV-B or *GAL10* particles (Table 2), which indicates that 5S particles have a greater stability. This is consistent with the larger fraction of high-FRET molecules in 5S populations (Fig. 3). The relative

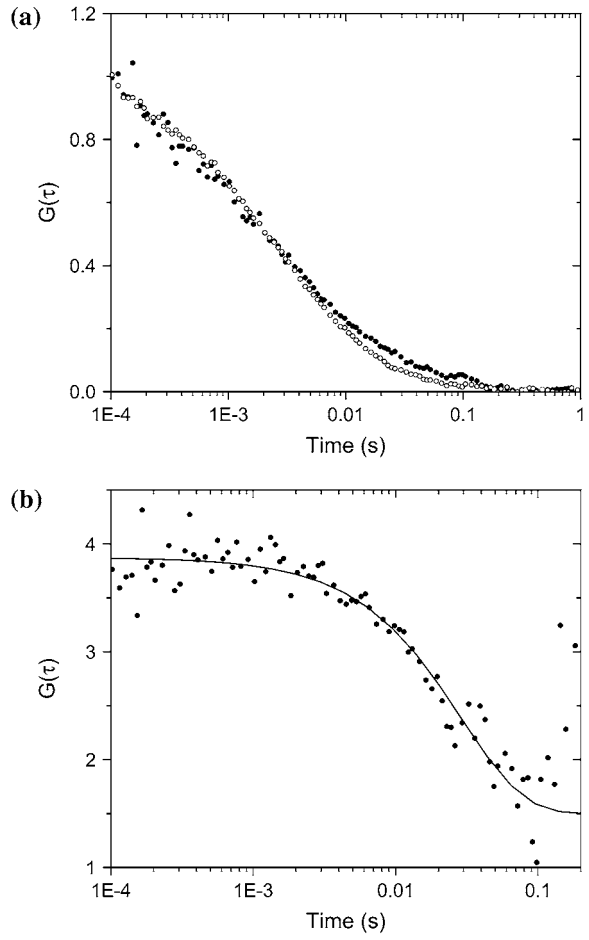

FIGURE 5 An FCS experiment to determine DNA dynamics. Panel *a* shows normalized donor autocorrelation curves obtained using single-labeled (*solid circles*) or double-labeled (*open circles*) MMTV-B particles embedded in 3% (w/v) agarose gels. In panel *b*, the filled circles show the experimentally determined ratios between the autocorrelation signals shown in panel *a*. The *x* axis shows lag time and the *y* axis is the normalized amplitude of the autocorrelation function. The solid curve represents a fit to the experimental data using Eq. S4 (Supplementary Material).

magnitudes of these three particle equilibrium constants, 5S > MMTV-B > *GAL10*, are consistent with the relative extents of FRET decrease produced at sub-nM concentrations, 5S < MMTV-B < *GAL10* ((42); Fig. 2). Equilibrium constants for formation of the closed state in intact nucleosomes show the same relative values, 5S > MMTV-B > *GAL10*, as for the corresponding particles (Table 2), indicating the central role of the tetramer in determining nucleosome stability. Our 5S K_{eq} value seems reasonable; 601 nucleosomes have a K_{eq} of 5–20 (38) but 601 DNA binds histones ~100-fold more strongly than does the 5S sequence (61).

The rate data provide some novel insights. k_{conf} is the sum of the forward and reverse reaction rate constants, i.e., the rate constants that describe the transit of particles between the open and closed conformational states. 5S particles exhibit somewhat higher reaction rates than MMTV-B and

TABLE 2 DNA dynamics: on/off rates estimated by FCS

Particle Type	K^{*}_{equil}	$k^{\dagger}_{conf}$, (s^{-1})	$\tau^{\ddagger}_{open}$, (ms)	$\tau^{\ddagger}_{closed}$, (ms)	$K^{\S}_{equil}$
5S	1.20 ± 0.14¶	54 ± 8	34 ± 7	41 ± 8	1.20 ± 0.12
MMTV	0.69 ± 0.08	42 ± 14	58 ± 19	40 ± 13	1.00 ± 0.10
GAL10	0.44 ± 0.05	40 ± 10	82 ± 22	36 ± 10	0.73 ± 0.07

*Equilibrium constants for particles at sub-nM concentrations.
†Calculated by fitting Eq. S4 (Supplementary Material) to the experimental data.
‡Calculated using Eq. S5 (Supplementary Material) and $\tau_{closed} = 1/k_{12}$, $\tau_{open} = 1/k_{21}$.
§Equilibrium constants for nucleosomes, calculated from bulk fluorescence spectra.
¶Mean ± SE.

GAL10 particles, whose rates are comparable to one another. τ_{open} and τ_{closed} are the times that the particle remains in the open (unwrapped) and closed (wrapped) states, respectively. The main difference among the three types of particles lies in τ_{open}, with τ_{closed} being similar in all three cases. The values indicate that 5S particles spend an almost equal amount of time in the open and closed states; MMTV-B particles spend ~50% longer and *GAL10* particles more than twice as long in the open as in the closed state. Thus, these three particles differ significantly in their residence times in the state in which the donor and acceptor are too far apart to give strong energy transfer. These inherent DNA dynamics differences are also consistent with the single-molecule population data, 5S versus the promoter particles (Fig. 3).

A previous FCS study (38) reported similar open residence times (at least for the 5S particle), ~10–50 ms, but much longer closed residence times, ~250 ms, than we observe. However, those studies used intact nucleosomes (100 nM concentration), reconstituted on 601 DNA, a synthetic sequence that forms more stable nucleosomes and binds histones much more strongly than 5S DNA does (61). Both features would be expected to enhance residence time in the closed state for the 601 nucleosome. Thus, these differences in closed residence times are understandable. In a single-molecule study of surface-attached complexes (39), the time resolution achieved was insufficient to allow a comparison with our values, but we note that at the concentrations typically used in surface single-molecule studies, nucleosomes are likely to be H2A/H2B depleted, based on our results (see above) and others (50).

DISCUSSION

This work continues our use of fluorescence-based FRET approaches in studies of nucleosome features (see also Kelbauskas et al. (42) and Lovullo et al. (43)). In these studies, DNA fragments ~160 bp in length are labeled with Cy3 and Cy5 at sites 80 bp apart (and roughly equidistant from each DNA terminus). Reconstitution of the labeled fragments into nucleosomes brings the donor and acceptor fluorophores close together, producing strong FRET signals (Fig. 1). Nucleosome conformational changes are detected as changes (usually decreases) in FRET levels.

Three types of labeled nucleosomal particles have been compared. *GAL10* and MMTV-B contain the TATA (*GAL10*) or hormone response elements (MMTV-B) from their respective promoters and are of interest because the nucleosomes covering these sequences in vivo undergo conformational transitions that play crucial roles in the gene activation process (44,45,62). The widely used sea urchin 5S rDNA nucleosome (46,63) provides a standard for comparison.

The DNA fragments are chosen to contain the major nucleosome position for each sequence (5S (49), MMTV-B (47,64), *GAL10* (44)) and labeled so that the probes will bracket the center and thus lie within the (positioned) nucleosome formed on the fragment (Fig. 1; see also (42)). Each of the three sequences forms typical nucleosomes, based on gel and salt stability analyses, and for each, a single-nucleosome position is observed (42). Note that these internal labels provide a different view of nucleosome conformational features (L. Kelbauskas, N. Chan, R. Bash, P. DeBartolo, J. Sun, N. Woodbury, and D. Lohr, manuscript in preparation) than do the more commonly used terminal labels (22,23,36–38,40,41).

Several FRET response differences reflecting structure or stability variations between 5S and the two promoter nucleosomes were detected previously (42), but the differences observed when nucleosomes were diluted to sub-nM concentrations were of special interest. These response variations could, in principle, arise simply from differences in intrinsic DNA features between 5S and the two promoter sequences, such as twist variations (cf. (65)), DNA bending differences (cf. (44)), or other sequence-associated features (cf. (26)). However, there is no evidence for a concentration-dependent transition involving any of those features nor is there an obvious reason why dilution should affect such (inherently intramolecular) features. On the other hand, these sub-nM concentrations are 50-fold lower than the concentrations shown previously to produce major H2A/H2B release in reconstituted nucleosomes (50), and a multimolecular process like H2A/H2B dissociation from the nucleosome should be concentration dependent. Thus, it is likely that these (100–200 pM) conditions produce H2A/H2B depletion and the differing FRET responses among the three types of nucleosomes involve varying effects associated with, or caused by, H2A/H2B release. The known role of DNA in stabilizing H3/H4 tetramer-H2A/H2B dimer associations in the octamer (1) opens up the possibility of DNA sequence-dependence contributions to that association.

In this work, a very different method—treatment with yNAP-1—was used to produce H2A/H2B release from nucleosomes. yNAP-1 is a histone chaperone that has been shown to cause H2A/H2B release from nucleosomes in vitro (19). yNAP-1 treatment produced the same FRET response differences as did dilution, decreases in MMTV-B and *GAL10* but not in 5S nucleosomes (Fig. 2 *a*). Moreover, the

extents of FRET decrease produced in MMTV-B and *GAL10* nucleosomes were quantitatively similar in both cases. Salt stability analyses showed that yNAP-1 treatment altered the stability of 5S nucleosomes. Thus yNAP-1 was acting on them, to apparently similar extents as for MMTV-B and *GAL10* nucleosomes (Fig. 2 *c*), even though the 5S nucleosomes exhibited no FRET change. The yNAP-1 results demonstrate clearly that differing FRET responses (5S versus MMTV-B or *GAL10* nucleosomes) result from H2A/H2B release, thus further strengthening the similar conclusion from dilution studies (42). These FRET response differences are DNA sequence-dependent effects since the studies were otherwise identical in all aspects (histones, labels, analysis techniques etc.).

Two possible explanations of how H2A/H2B release (at sub-nM concentrations) could produce FRET response variations among these three types of nucleosomes were previously discussed (42). They are as follows: 1) differences in the amounts of H2A/H2B released, and 2) differences in how H2A/H2B release affects the residual (depleted) nucleosome. According to explanation 1, 5S FRET does not change because 5S nucleosomes maintain significantly more H2A/H2B at these sub-nM concentrations than do MMTV-B and *GAL10* nucleosomes. Explanation 2 would posit that all three types of nucleosomes lose H2A/H2B, probably to significant (and perhaps similar) extents, but H2A/H2B-depleted 5S complexes are better able to keep the fluorophores close, and thus maintain a high FRET efficiency, compared to depleted MMTV-B or *GAL10* nucleosomes. We note that our probes should lie in the DNA regions contacted by H2A/H2B in intact nucleosomes but close to the H3/H4 tetramer-DNA contact regions (cf. Fig. 1).

It seems unlikely that differing amounts of H2A/H2B remaining in these complexes at sub-nM concentrations could account entirely for the FRET response variations. MMTV-B and *GAL10* FRET efficiencies drop steadily below ~2 nM (42). Assuming that these steady FRET decreases reflect increasing H2A/H2B loss, the complete absence of any decrease for 5S nucleosomes by 100 pM concentrations would require that 5S nucleosomes have not even begun to lose H2A/H2B at concentrations that are 50-fold lower than those shown previously to produce extensive H2A/H2B release from reconstituted nucleosomes (50) and 20-fold lower than the concentrations at which MMTV-B and *GAL10* nucleosomes begin to lose H2A/H2B. Unfortunately, the very low concentrations at which these FRET changes occur preclude the use of sedimentation or even gel analyses, which were used in previous studies to test quantitatively for H2A/H2B release (19,50). Therefore, the possibility that there are differences in the residual amounts of H2A/H2B in these three cannot be completely excluded at this time.

Several observations support option 2, namely that the FRET variations observed at these sub-nM concentrations reflect differences in the ability of H2A/H2B loss to affect the average fluorophore separation in the depleted complexes. First, the yNAP-1 results show that differential FRET responses are observed (Fig. 2 *a*) in nucleosomes that appear to be H2A/H2B depleted to similar extents (Fig. 2, *b* and *c*). Second, heating nucleosomes to ~40°C, which loosens the terminal 20 or so bp of DNA (66), causes FRET decreases in MMTV-B and *GAL10* but not in 5S particles (42), again demonstrating that these three particles differ in the extents to which changes in distal regions affect the internal regions (where our fluorophores are located). Third, two-state behavior and similar closed times (Table 2) for the three particles argue that they are compositionally similar (see Results) and thus indirectly support explanation 2.

5S DNA is one of the strongest natural histone-binding DNA sequences known (25,61) and binds histone octamers more strongly than does MMTV promoter DNA (35). These exceptionally strong binding properties could be responsible for the ability of depleted 5S nucleosomes to keep the fluorophores in close contact (and thus undergo no FRET change during H2A/H2B depletion). The maintenance of stronger DNA-histone binding in 5S particles is consistent with the similar values for 5S nucleosome and particle equilibrium constants (but not for MMTV-B or *GAL10*) and with the lower level of DNA dynamics in 5S compared to MMTV-B and *GAL10* particles (Table 2). 5S DNA binds strongly to H3/H4 tetramers (67), which is also consistent with the maintenance of strong binding in H2A/H2B-depleted particles. It has been suggested that H3/H4 tetramers can bind up to a full nucleosomal length of DNA (cf. (67)). Thus, DNA released as a result of H2A/H2B loss could maintain contacts with the tetramer.

For the above reasons, we favor the explanation that the main cause of the differing FRET responses as nucleosomes are diluted to sub-nM concentrations (or treated with yNAP-1) is a difference in the ability of H2A/H2B loss to affect DNA-histone binding in the depleted nucleosome. Rate data indicate that these differences may involve DNA dynamics differences. Such differences suggest that H2A/H2B loss implemented by the action of various transcription-associated complexes like FACT (16), ATP-dependent nucleosome remodeling complexes (17,18), or RNA polymerase (15) could have differing effects on nucleosomes, producing more significant destabilization in some (cf. MMTV-B/*GAL10*) compared to others (cf. 5S). Such differences could make the former types more amenable to further disruption or, since the differences apparently are associated with differing DNA dynamics in the central regions of the nucleosome (Table 2), could lead to differing accessibilities of this DNA. The emerging role of H2A/H2B release in transcription-associated processes (see above) and the inherent dynamics of H2A/H2B in vivo (14) make further studies of these types of effects of great interest.

Although both promoter nucleosomes respond to H2A/H2B depletion in a quite different way than 5S, the MMTV-B and *GAL10* responses are not identical; MMTV-B FRET decreases are more modest, whether depleted by yNAP-1

(see Results) or dilution (42), suggesting that H2A/H2B depletion produces lower levels of destabilization in MMTV-B than in *GAL10* particles. This is consistent with the enhanced DNA dynamics in *GAL10* particles (Table 2). Thus, there may be a diverse set of individual nucleosome variations with respect to these types of stability and dynamics effects. The results presented here and previously (42) suggest that to uncover the full range of nucleosomal features, especially for biologically relevant nucleosomes (see also Giresi et al. (20)), it will be necessary to study many types of nucleosomes, not just those reconstituted on the very strongly positioning DNA sequences, natural or artificial.

SUPPLEMENTARY MATERIAL

To view all of the supplemental files associated with this article, visit www.biophysj.org.

We thank Dr. K. Luger and Dr. Y. Park for yNAP-1 and valuable discussions.

This work was supported by National Science Foundation Grants PHY-0239986 (to N.W. and D.L.), PHY-0631631 (to N.W.), National Institutes of Health Grant Ca 85990 (to D.L.), and Science Foundation of Arizona Grant CAA 0122-07 (to N.W.).

REFERENCES

1. Van Holde, K., J. Zlatanova, G. Arents, and E. Moudrianakis. 1995. Elements of chromatin structure: histones, nucleosomes, fibers. *In* Chromatin Structure and Gene Expression. S. C. Elgin, editor. Oxford University Press, Oxford, UK. 1–21.
2. Luger, K., A. W. Mader, R. K. Richmond, D. F. Sargent, and T. J. Richmond. 1997. Crystal structure of the nucleosome core particle at 2.8 Å resolution. *Nature*. 18:251–260.
3. Lohr, D., R. T. Kovacic, and K. E. Van Holde. 1977. Quantitative analysis of the digestion of yeast chromatin by staphylococcal nuclease. *Biochemistry*. 16:463–471.
4. Bernstein, B. E., C. L. Liu, E. L. Humphrey, E. O. Perlstein, and S. L. Schreiber. 2004. Global nucleosome occupancy in yeast. *Genome Biol*. 5:R62.1–R62.11.
5. Hager, G., C. Smith, T. Svaren, and W. Hortz. 1995. Initiation of Expression: Remodeling Genes. Oxford University Press, Oxford, UK.
6. Lohr, D. 1997. Nucleosome transactions on the promoters of the yeast GAL and PHO genes. *J. Biol. Chem*. 272:26795–26798.
7. Huebert, D. J., and B. E. Bernstein. 2005. Genomic views of chromatin. *Curr. Opin. Genet. Dev*. 15:476–481.
8. Sogo, J. M., H. Stahl, T. Koller, and R. Knippers. 1986. Structure of replicating simian virus 40 minichromosomes. The replication fork, core histone segregation and terminal structures. *J. Mol. Biol*. 189:189–204.
9. Lohr, D., and T. Torchia. 1988. Structure of the chromosomal copy of yeast ARS1. *Biochemistry*. 27:3961–3965.
10. Luger, K., and J. C. Hansen. 2005. Nucleosome and chromatin fiber dynamics. *Curr. Opin. Struct. Biol*. 15:188–196.
11. Luger, K. 2003. Structure and dynamic behavior of nucleosomes. *Curr. Opin. Genet. Dev*. 13:127–135.
12. Luger, K. 2006. Dynamic nucleosomes. *Chromosome Res*. 14:5–16.
13. Sharma, S., F. Ding, and N. V. Dokholyan. 2007. Multiscale modeling of nucleosome dynamics. *Biophys. J*. 92:1457–1470.
14. Kimura, H., and P. R. Cook. 2001. Kinetics of core histones in living human cells: little exchange of H3 and H4 and some rapid exchange of H2B. *J. Cell Biol*. 153:1341–1353.
15. Studitsky, V. M., W. Walter, M. Kireeva, M. Kashlev, and G. Felsenfeld. 2004. Chromatin remodeling by RNA polymerases. *Trends Biochem. Sci*. 29:127–135.
16. Reinberg, D., and R. J. Sims. 2006. de FACTo nucleosome dynamics. *J. Biol. Chem*. 281:23297–23301.
17. Bruno, M., A. Flaus, C. Stockdale, C. Rencurel, H. Ferreira, and T. Owen-Hughes. 2003. Histone H2A/H2B dimer exchange by ATP-dependent chromatin remodeling activities. *Mol. Cell*. 12:1599–1606.
18. Bash, R., H. Wang, C. Anderson, J. Yodh, G. Hager, S. M. Lindsay, and D. Lohr. 2006. AFM imaging of protein movements: histone H2A–H2B release during nucleosome remodeling. *FEBS Lett*. 580: 4757–4761.
19. Park, Y. J., J. V. Chodaparambil, Y. H. Bao, S. J. McBryant, and K. Luger. 2005. Nucleosome assembly protein 1 exchanges histone H2A–H2B dimers and assists nucleosome sliding. *J. Biol. Chem*. 280:1817–1825.
20. Giresi, P. G., M. Gupta, and J. D. Lieb. 2006. Regulation of nucleosome stability as a mediator of chromatin function. *Curr. Opin. Genet. Dev*. 16:171–176.
21. Khorasanizadeh, S. 2004. The nucleosome: from genomic organization to genomic regulation. *Cell*. 116:259–272.
22. Park, Y. J., P. N. Dyer, D. J. Tremethick, and K. Luger. 2004. A new fluorescence resonance energy transfer approach demonstrates that the histone variant H2AZ stabilizes the histone octamer within the nucleosome. *J. Biol. Chem*. 279:24274–24282.
23. Bao, Y., K. Konesky, Y. J. Park, S. Rosu, P. N. Dyer, D. Rangasamy, D. J. Tremethick, P. J. Laybourn, and K. Luger. 2004. Nucleosomes containing the histone variant H2A.Bbd organize only 118 base pairs of DNA. *EMBO J*. 23:3314–3324.
24. Black, B. E., D. R. Foltz, S. Chakravarthy, K. Luger, V. L. Woods, and D. W. Cleveland. 2004. Structural determinants for generating centromeric chromatin. *Nature*. 430:578–582.
25. Shrader, T. E., and D. M. Crothers. 1990. Effects of DNA sequence and histone-histone interactions on nucleosome placement. *J. Mol. Biol*. 216:69–84.
26. Widom, J. 2001. Role of DNA sequence in nucleosome stability and dynamics. *Q. Rev. Biophys*. 34:269–324.
27. Wu, C., and A. Travers. 2005. Relative affinities of DNA sequences for the histone octamer depend strongly upon both the temperature and octamer concentration. *Biochemistry*. 44:14329–14334.
28. Krajewski, W. A. 2002. Histone acetylation status and DNA sequence modulate ATP-dependent nucleosome repositioning. *J. Biol. Chem*. 277:14509–14513.
29. Vicent, G. P., A. S. Nacht, C. L. Smith, C. L. Peterson, S. Dimitrov, and M. Beato. 2004. DNA instructed displacement of histones H2A and H2B at an inducible promoter. *Mol. Cell*. 16:439–452.
30. Anderson, J. D., and J. Widom. 2000. Sequence and position-dependence of the equilibrium accessibility of nucleosomal DNA target sites. *J. Mol. Biol*. 296:979–987.
31. Widlund, H. R., J. M. Vitolo, C. Thiriet, and J. J. Hayes. 2000. DNA sequence-dependent contributions of core histone tails to nucleosome stability: differential effects of acetylation and proteolytic tail removal. *Biochemistry*. 39:3835–3841.
32. Gemmen, G. J., R. Sim, K. A. Haushalter, P. C. Ke, J. T. Kadonaga, and D. E. Smith. 2005. Forced unraveling of nucleosomes assembled on heterogeneous DNA using core histones, NAP-1, and ACF. *J. Mol. Biol*. 351:89–99.
33. Babendure, J., P. A. Liddell, R. Bash, D. LoVullo, T. K. Schiefer, M. Williams, D. C. Daniel, M. Thompson, A. K. W. Taguchi, D. Lohr, and N. W. Woodbury. 2003. Development of a fluorescent probe for the study of nucleosome assembly and dynamics. *Anal. Biochem*. 317:1–11.
34. Gottesfeld, J. M., C. Melander, R. K. Suto, H. Raviol, K. Luger, and P. B. Dervan. 2001. Sequence-specific recognition of DNA in the nucleosome by pyrrole-imidazole polyamides. *J. Mol. Biol*. 309: 615–629.

35. Solis, F., R. Bash, H. Wang, J. Yodh, S. Lindsay, and D. Lohr. 2007. Properties of nucleosomes in acetylated mouse mammary tumor virus vs. 5S arrays. *Biochemistry*. 46:5623–5636.

36. Toth, K., N. Brun, and J. Langowski. 2001. Trajectory of nucleosomal linker DNA studied by fluorescence resonance energy transfer. *Biochemistry*. 40:6921–6928.

37. White, C. L., and K. Luger. 2004. Defined structural changes occur in a nucleosome upon Amt1 transcription factor binding. *J. Mol. Biol.* 342:1391–1402.

38. Li, G., M. Levitus, C. Bustamante, and J. Widom. 2005. Rapid spontaneous accessibility of nucleosomal DNA. *Nat. Struct. Mol. Biol.* 12: 46–53.

39. Tomschik, M., H. Zheng, K. van Holde, J. Zlatanova, and S. H. Leuba. 2005. Fast, long-range, reversible conformational fluctuations in nucleosomes revealed by single-pair fluorescence resonance energy transfer. *Proc. Natl. Acad. Sci. USA*. 102:3278–3283.

40. Bussiek, M., K. Toth, N. Schwarz, and J. Langowski. 2006. Trinucleosome compaction studied by fluorescence energy transfer and scanning force microscopy. *Biochemistry*. 45:10838–10846.

41. Toth, K., N. Brun, and J. Langowski. 2006. Chromatin compaction at the mononucleosome level. *Biochemistry*. 45:1591–1598.

42. Kelbauskas, L., N. Chan, R. Bash, J. Yodh, N. Woodbury, and D. Lohr. 2007. Sequence-dependent nucleosome structure and stability variations detected by Förster resonance energy transfer. *Biochemistry*. 46:2239–2248.

43. Lovullo, D., D. Daniel, J. Yodh, D. Lohr, and N. W. Woodbury. 2005. A fluorescence resonance energy transfer-based probe to monitor nucleosome structure. *Anal. Biochem.* 341:165–172.

44. Bash, R., and D. Lohr. 2001. Yeast chromatin structure and regulation of GAL gene expression. *Prog. Nucleic Acid Res. Mol. Biol.* 65: 197–259.

45. Hager, G. L. 2001. Understanding nuclear receptor function: from DNA to chromatin to the interphase nucleus. *Prog. Nucleic Acid Res. Mol. Biol.* 66:279–305.

46. Hansen, J. C. 2002. Conformational dynamics of the chromatin fiber in solution: determinants, mechanisms, and functions. *Annu. Rev. Biophys. Biomol. Struct.* 31:361–392.

47. Fragoso, G., S. John, M. S. Roberts, and G. L. Hager. 1995. Nucleosome positioning on the MMTV LTR results from the frequency-biased occupancy of multiple frames. *Genes Dev.* 9:1933–1947.

48. Flaus, A., and T. J. Richmond. 1998. Positioning and stability of nucleosomes on MMTV 3′LTR sequences. *J. Mol. Biol.* 275:427–441.

49. Dong, F., J. C. Hansen, and K. E. van Holde. 1990. DNA and protein determinants of nucleosome positioning on sea urchin 5S rRNA gene sequences in vitro. *Proc. Natl. Acad. Sci. USA*. 87:5724–5728.

50. Claudet, C., D. Angelov, P. Bouvet, S. Dimitrov, and J. Bednar. 2005. Histone octamer instability under single molecule experiment conditions. *J. Biol. Chem.* 280:19958–19965.

51. Fletcher, T. M., B. W. Ryu, C. T. Baumann, B. S. Warren, G. Fragoso, S. John, and G. L. Hager. 2000. Structure and dynamic properties of a glucocorticoid receptor-induced chromatin transition. *Mol. Cell. Biol.* 20:6466–6475.

52. Bash, R. C., J. Yodh, Y. Lyubchenko, N. Woodbury, and D. Lohr. 2001. Population analysis of subsaturated 172–12 nucleosomal arrays by atomic force microscopy detects nonrandom behavior that is favored by histone acetylation and short repeat length. *J. Biol. Chem.* 276: 48362–48370.

53. Yodh, J. G., Y. L. Lyubchenko, L. S. Shlyakhtenko, N. Woodbury, and D. Lohr. 1999. Evidence for nonrandom behavior in 208–12 subsaturated nucleosomal array populations analyzed by AFM. *Biochemistry*. 38:15756–15763.

54. Magde, D., W. W. Webb, and E. Elson. 1972. Thermodynamic fluctuations in a reacting system—measurement by fluorescence correlation spectroscopy. *Phys. Rev. Lett.* 29:705–708.

55. Berne, B. J., and R. Pecora. 1976. Dynamic Light Scattering. Wiley, New York.

56. Krichevsky, O., and G. Bonnet. 2002. Fluorescence correlation spectroscopy: the technique and its applications. *Rep. Prog. Phys.* 65:251–297.

57. Bonnet, G., O. Krichevsky, and A. Libchaber. 1998. Kinetics of conformational fluctuations in DNA hairpin-loops. *Proc. Natl. Acad. Sci. USA*. 95:8602–8606.

58. Pennings, S. 1999. Nucleoprotein gel assays for nucleosome positioning and mobility. *Methods Enzymol.* 304:298–312.

59. Luger, K. J. R., and T. J. Richmond. 1999. Expression and purification of recombinant histones and nucleosome reconstitution. *Methods Mol. Biol.* 119:1–16.

60. Czarnota, G. J., and F. P. Ottensmeyer. 1996. Structural states of the nucleosome. *J. Biol. Chem.* 271:3677–3683.

61. Thastrom, A., P. T. Lowary, H. R. Widlund, H. Cao, M. Kubista, and J. Widom. 1999. Sequence motifs and free energies of selected natural and non-natural nucleosome positioning DNA sequences. *J. Mol. Biol.* 288:213–229.

62. Lohr, D. 1984. Organization of the GAL1–GAL10 intergenic control region chromatin. *Nucleic Acids Res.* 12:8457–8474.

63. Simpson, R. T., and D. W. Stafford. 1983. Structural features of a phased nucleosome core particle. *Proc. Natl. Acad. Sci. USA*. 80:51–55.

64. Fragoso, G., W. D. Pennie, S. John, and G. L. Hager. 1998. The position and length of the steroid-dependent hypersensitive region in the mouse mammary tumor virus long terminal repeat are invariant despite multiple nucleosome B frames. *Mol. Cell. Biol.* 18:3633–3644.

65. Edayathumangalam, R. S., P. Weyermann, P. B. Dervan, J. M. Gottesfeld, and K. Luger. 2005. Nucleosomes in solution exist as a mixture of twist-defect states. *J. Mol. Biol.* 345:103–114.

66. Van Holde, K. 1989. Chromatin. Springer Verlag, New York, NY.

67. Dong, F., and K. E. Van Holde. 1991. Nucleosome positioning is determined by the (H3–H4)2 tetramer. *Proc. Natl. Acad. Sci. USA*. 88:10596–10600.